

# Geochemistry, Geophysics, Geosystems

## RESEARCH ARTICLE

10.1029/2017GC007352

### Key Points:

- The weathering intensity index was generated from gamma ray and relief data for the Brazilian Amazon
- A lateritic index was created to determine favorable areas for the presence of lateritic duricrusts in the Brazilian Amazon
- A regolith map was created using field data integrated with geophysics and geochemistry

### Supporting Information:

- Supporting Information S1
- Table S1

### Correspondence to:

E. R. H. F. Iza,  
edgar.iza@cprm.gov.br

### Citation:


Iza, E. R. H. F., Horbe, A. M. C., Castro, C. C., & Herrera, I. L. I. E. (2018). Integration of geochemical and geophysical data to characterize and map lateritic regolith: An example in the Brazilian Amazon. *Geochemistry, Geophysics, Geosystems*, 19. <https://doi.org/10.1029/2017GC007352>

Received 27 NOV 2017

Accepted 24 JUL 2018

Accepted article online 18 AUG 2018

## Integration of Geochemical and Geophysical Data to Characterize and Map Lateritic Regolith: An Example in the Brazilian Amazon

E. R. H. F. Iza<sup>1,2</sup> , A. M. C. Horbe<sup>2</sup>, C. C. Castro<sup>3</sup>, and I. L. I. E. Herrera<sup>4</sup>

<sup>1</sup>Serviço Geológico do Brasil-CPRM, Salvador, Brazil, <sup>2</sup>Instituto de Geociências, Universidade de Brasília-UnB, Campus Universitário Darcy Ribeiro, Brasília, Brazil/CNPq, <sup>3</sup>Serviço Geológico do Brasil-CPRM, Belo Horizonte, Brazil, <sup>4</sup>Universidade Federal de Rondônia-UNIR, Programa de Pós-Graduação em Geografia, PPGG, Porto Velho, Brazil

**Abstract** In tropical regions like the Amazon, there are extensive lateritic covers that have not been properly mapped, despite their economic-bearing minerals and their importance related to denudation and regolith landscape studies. To consolidate tools for regolith cartography, geochemical and geophysical data (airborne gamma ray spectrometry and magnetometry) were integrated. Regional indexes (including the weathering intensity index, WII; lateritic index, LI; and mafic index, MI) were generated and applied, which allowed for the identification of regolith properties. The WII highlighted areas with high weathering levels located between 149 and 300 m and between 500 and 627 m of altitude that are related to the lower planation surface and upper planation surfaces, respectively. The LI ratified the WII and highlighted areas with high Th/K and U/K ratios, associated with lateritic duricrusts. The correlation between LI and MI showed lateritic duricrusts related to mafic and felsic substrates, especially on altitudes below 300 m, which confirmed the geochemical data. All of these results lead to the reinterpretation of areas previously considered to be sedimentary as residuals associated with oxisols and lateritic duricrusts, and this allows us to propose that the regolith mapping techniques and model generation (weathering intensity and lateritic indexes) have a good level of reliability.

### 1. Introduction

The application of gamma ray spectrometric data using mathematical techniques integrated with geology and altimetry has increasingly contributed to the development of mapping techniques used to interpret geomorphological and weathering processes (Arhin et al., 2015; Carranza, 2009; McBratney et al., 2003; Moreira et al., 2003; Wilford, 2012; Wilford et al., 1997). Wilford (2012), for example, developed the weathering intensity index (WII) for Australia using gamma ray spectrometric and altimetric data and obtained excellent results at a regional scale defining areas with different levels of weathering. Other authors confirm that high values of U and Th (from aero geophysical data), often above the Earth's crustal average, together with low values of K, identify lateritic products (such as lateritic duricrust, gossan, and bauxites) and their respective parent rocks (Barbosa et al., 2013; Carrier et al., 2006; Carrino et al., 2011; Dauth, 1997; Dickson & Scott, 1997; Isles & Rankin, 2000; Iza et al., 2016). On the other hand, Minty (2011) states that radiometric ratios tend to remove environmental artifacts related to humidity and vegetation. These results make gamma ray spectrometry a useful and reliable tool for regolith studies.

Strangely, regolith mapping supported by multisource techniques has been developed for decades. For example, in Australia, it has contributed not only to understanding landscape evolution but also to the determination of true or false geochemical anomalies. To understand the distribution of residual soils, transported soils, lateritic duricrusts, colluvium, and any regolithic material, both geochemical and geophysical interpretations are used. Cohen et al. (2010) highlight that, in complex regolith terrains, residual anomalies can be distinguished from transported anomalies by matching the regolith map with surface geochemical data. Anand and Paine (2002) show that thick regolith can have a large impact on mineral exploration (because of difficulty recognizing parent lithology, spurious enrichment of target elements in weathered and unmineralized rocks, complex geochemical signatures masked by transported sediments, and development of false anomalies). These authors state that mapping the regolith is important since it helps to assess the origin of the regolith, geomorphological processes, styles of weathering, and regolith-landform relationships. Despite the importance and benefits of the regolith

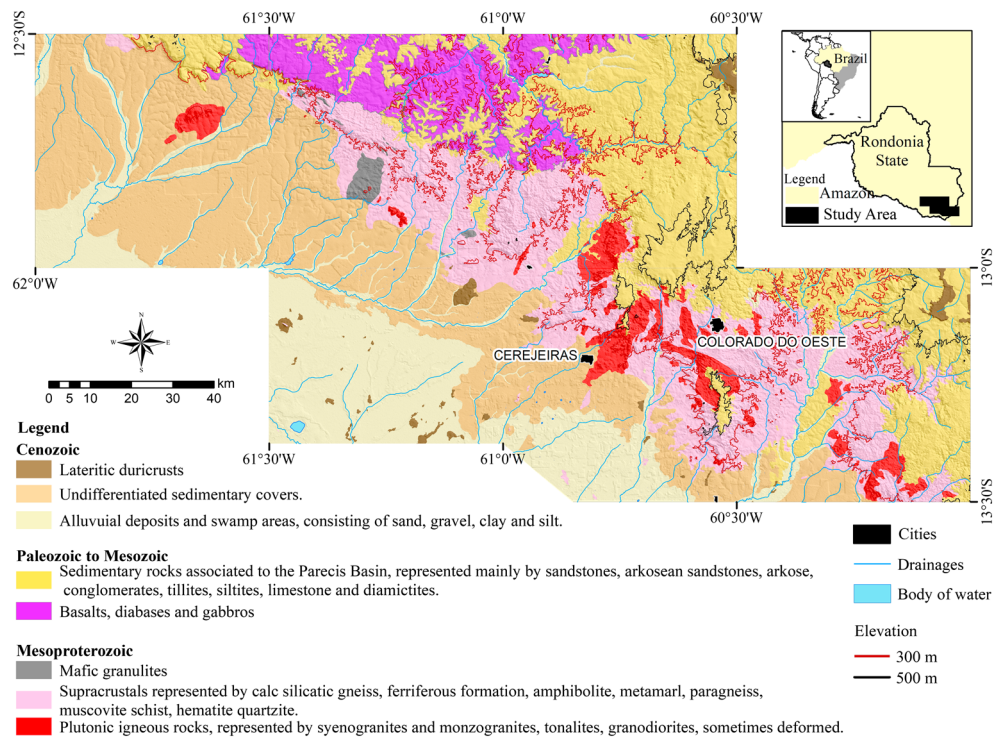


**Figure 1.** Simplified geologic map of the area, modified from Quadros et al. (2007).

map, the authors state that it is still not a routine procedure for exploration programs. This is even truer in Brazil.

Approximately 65% of Brazil is covered by lateritic regolith, with important supergene mineral deposits, especially in the Amazon (e.g., Albuquerque et al., 2017; Boulangé & Carvalho, 1997; Costa, 1997; Kotschoubey et al., 2005; Oliveira et al., 2016). However, multisource techniques for mapping the regolith have not yet been developed for the Amazon or applied widely and systematically. Anand and Paine (2002) suggest that an outline for regolith mapping should integrate multisource data sets such as airborne radiometrics, magnetics and electromagnetics, airborne radar, geological maps, and topographic maps. With this in mind, the current work is aimed to integrate multisource data in the geographic information system (GIS) environment, such as geophysics, geochemistry, geology and relief (Shuttle Radar Topography Mission, SRTM), supported by fieldwork, to characterize and map the lateritic regolith. The other objectives are

1. to compare and evaluate geophysical and geochemical data to characterize the regolith and understand the respective patterns (geophysical and geochemical) and eventual false anomalies; and
2. to develop and consolidate tools, such as the lateritic index (LI), the WII, and the mafic index (MI), to aid with the mapping of the regolith and respective interpretations.

## 2. Location, Geological, and Geomorphological Aspects

The study area is located in the southwest of the Brazilian Amazon, along the border of Bolivia, and has approximately 17,000 km<sup>2</sup>. The climate type is tropical rainy with precipitation between 1,400 and 2,600 mm/year (Brasil, 1979; Inpe, 2018). The area has three major geomorphologic domains according to Iza et al. (2016): (i) the upper planation surface (UPS), with altitudes between 500 and 627 m, associated with Mesozoic sedimentary rocks (Parecis basin) and Paleozoic mafic rocks covered by lateritic duricrusts; (ii) the lower planation surface (LPS), with altitudes below 300 m, locally limited by abrupt scarps and related to undifferentiated sedimentary covers, lateritic duricrusts, and recent deposits of clay, silt, sand, and gravel; at altitudes below 250 m, the low areas are frequently flooded, especially near rivers and lakes; and (iii) the Intermediate Zone (IZ), with altitudes between 301 and 499 m, with convex to sharp tops related to Mesoproterozoic mafic rocks, gneisses, schists, and granitoids (Figure 1).

**Table 1**  
*Classification of Regolith Level of Weathering for the Study Area (Modified From Wilford, 2012)*

Level (WC)	Weathering intensity	Descriptions
1	Unweathered	Unaltered rock with no signs of decomposition or discoloring. Rock outcrops are very common.
2	Slightly weathered	Rock slightly discolored with eventual staining. The overall fabric of the rock is well preserved, and outcrops are common. Soils are typically lithosols. Primary minerals are largely preserved; however, feldspars can be slightly weathered.
3	Moderately weathered	Residual sands and clays are common in the upper part of the weathering profile. Rock partially weathered but still cohesive. Most of the feldspars are weathered. Primary minerals still present, as well as smectite, kaolinite, and iron oxihydroxides. Outcrops are rare or absent.
4	Highly weathered	Residual sands and clays are common in the upper part of the weathering profile. The fabric of the rock is weakly preserved. Saprolite commonly mottled and ferruginous. The material can be broken by hand. The mineral content is dominated by clays, quartz, and oxihydroxides, and the principle primary minerals, such as feldspars, are weathered. Minor outcrops frequently highly weathered.
5	Intensely weathered	Residual sands and clays are common in the upper part of the profile; mottling and leaching are intense and frequent. Lateritic duricrust and lateritic gravels are common. Saprolite is soft with primary minerals completely weathered to form clays or oxihydroxides. Quartz is the only remaining primary mineral, and quartz veins can still appear. The few outcrops are typically weathered and indurated by oxihydroxides.

Note. WC = weathering class.

### 3. Materials and Methods

The aero geophysical data were used as a tool to delimit areas with higher or lower weathering levels, which is useful for mapping the regolith. Geochemical data were compared with geophysical data, which contributed to the refinement of the cartography and the characterization of the regolith, and also to the determination of geochemical associations and of eventual anomalies (true or false). All of the interpretations and evaluations were performed in GIS, where each level of information (geophysics, geochemistry, geomorphology, altimetry, and field data) was integrated to form the final regolith map. All of the procedures performed are described in sections 3.1 and 3.2.

#### 3.1. Airborne Gamma Ray Spectrometry and Magnetometry

The gamma ray spectrometric and magnetometric data used in this paper were acquired by Fugro Airborne Surveys for the Brazilian Geological Survey (CPRM-Companhia de Pesquisa de Recursos Minerais) between 2005 and 2006 (Projeto Sudeste de Rondônia - Southeastern Rondônia Project, CPRM - Serviço Geológico do Brasil, 2006). The main products used were the dose, K, Th, U, and the Th/K and U/K ratios. The software used was Oasis Montaj 8.5 from Geosoft and ArcGIS 10.3 from Environmental Systems Research Institute, with the Geosoft extension, which permitted the processing of the aero geophysical images and management of all data, including altimetry SRTM data.

The gamma-spectrometric data were used to determine the main domains with high and low values of Th, U, and K, which aided in delimiting areas with higher or lower weathering, especially as defined by high ratios of Th/K and U/K. To make the evaluation of weathering more robust using gamma-spectrometric data, the WII of the area was developed, using the procedure from Wilford (2012), with some adaptations to fit the study area (Amazon context). The WII was calculated in three stages. First, we classified the regolith into five weathering classes (WCs) using data from 174 sites (Table 1). The WCs were divided according to the presence or absence of outcrops, preservation of the rock fabrics, proportion of clay minerals, and degree of mottling and ferruginization. Areas considered to be unweathered were those where rocky outcrops are predominant with rare signals of decomposition and no soil cover. The areas considered to be more intensely weathered and less

**Table 2**  
Basic Statistics

	N	Average	Minimum	Maximum	Standard deviation	Asymmetry
Altimetry	174	346.5	187.0	611.7	104.4	0.34
Dose	174	4.3	1.6	11.7	1.9	1.37
K	174	1.3	0.4	4.6	0.9	1.62
Th	174	6.8	1.0	22.0	4.3	1.48
U	174	1.2	0.0	2.8	0.5	0.41
ThK	174	10.8	1.9	51.1	8.6	1.59
U/K	174	10.1	1.7	21.7	5.1	0.33

eroded were those where lateritic duricrusts and soil covers are predominant (including the predominant presence of iron oxyhydroxides, such as goethite, gibbsite and hematite, and clay minerals, such as kaolinite). We also calculated statistical parameters (including average, maximum, minimum, standard deviation, and asymmetry) and performed correlation analysis, considering altimetry, Th, U, K, Th/K, U/K, and dose with the WCs (Table 2). The following correlation intervals ( $r$ ) were considered: *weak* (0 to  $\pm 0.29$ ), *regular* ( $\pm 0.3$  to  $\pm 0.79$ ), *strong* ( $\pm 0.8$  to  $\pm 0.89$ ), *very strong* ( $\pm 0.9$  to  $\pm 0.99$ ), and *perfect* ( $\pm 1$ ), and the results are shown in Table 3. Finally, we generated the regression equation and final WII map.

In the correlation phase, seven variables (altimetry, Th, U, K, Th/K, U/K, and dose) were considered and correlated with the WC derived from field data. Those variables with correlations between  $-0.5$  and  $0.5$  were discarded because they have low correlation with the weathering classes and, hence, have no mathematical importance. Thus, only the altimetry (SRTM), the K channel, and the Th/K and U/K ratios were used in the multiple regression procedure. The method of regression was the backward stepwise regression, which begins with all highly correlated variables, and according to the significance factor  $p$  ( $p < 0.05$ ), the variables are kept or removed, one by one, to obtain the best fit of the model.

After the first regression, despite the acceptable inverse correlation of K with WC ( $-0.70$ ); the significance factor for the variable was too high ( $p > 0.05$ ), which led to its removal from the regression process. After the second regression was performed with the remaining variables (SRTM, Th/K, and U/K),  $p$  values were less than  $0.05$ , indicating that the multiple regression equation has an overall strong significance and that it is statistically appropriate to use it for weathering predictions. The F statistic ratifies the significance of the regression, showing values above the critical limit calculated for the sample set (3.1161). This value was obtained based on the degrees of freedom (3 to 170) acquired on the calculation of the regression (Table 4). The result is the linear regression shown in equation (1):

$$WII = 2.2688 - 0.003 * SRTM + 0.411 * Th/K + 0.167 * U/K, \quad (1)$$

where WII is the weathering intensity index of the area.

**Table 3**  
Pearson Correlation Coefficient Results

	WC	Altimetry <sup>a</sup>	Dose	K	Th	U	Th/K	U/K
WC	1.00	<b>-0.51</b>	-0.29	<b>-0.70</b>	0.32	0.08	<b>0.71</b>	<b>0.82</b>
Altimetry <sup>a</sup>		1.00	0.25	0.35	-0.01	-0.02	-0.26	-0.38
Dose			1.00	0.67	0.59	0.28	0.09	-0.40
K				1.00	-0.06	-0.08	-0.58	-0.82
Th					1.00	0.13	0.72	0.25
U						1.00	0.15	0.16
Th/K							1.00	0.77
U/K								1.00

Note. WC = weathering class described in Table 1. SRTM = Shuttle Radar Topography Mission.  
<sup>a</sup>From SRTM data.

**Table 4**  
Summary of Stepwise Regression

	Variables included	Multiple R	Multiple R squared	F statistic	P level
Altimetry <sup>a</sup>	1	0.5035	0.2535	58.3975	0.0000
Th/K	2	0.7856	0.6172	137.8591	0.0003
U/K	3	0.8566	0.7337	156.1413	0.0000

Note. SRTM = Shuttle Radar Topography Mission.  
<sup>a</sup>From SRTM data.

In the next stage, altimetric (SRTM) and gamma ray spectrometric images (Th/K and U/K) were used in the weathering equation (WII) through map algebra in ArcGIS software to obtain the final WII map. The WII was later correlated with geochemical data to understand the weathering patterns and other associations (such as geomorphology and landscape evolution).

The LI developed in this paper is used to highlight the favorable areas for the occurrence of lateritic duricrusts, which were determined based on the direct relationship between the WC and the Th/K and U/K ratios (Table 3), according to equation (2):

$$LI = (eTh/K) \times (eU/K) = (eTh \times eU) / K^2. \quad (2)$$

The MI (MI = ASA/(K\*U\*Th; Pires & Moraes, 2006) was applied to differentiate parent rocks of lateritic duricrusts (basic rocks versus acidic rocks). The ASA (analytic signal amplitude) was calculated through the combination of horizontal (dx and dy) and vertical (dz) first-order derivatives of the magnetic anomaly (equation (3)) and is independent from the magnetization direction or the Earth's magnetic field direction (Roest et al., 1992). Horizontal derivatives highlight the eventual sources of the anomalies, while vertical derivatives amplify the short wavelength in detriment of the long wavelength. The denominator of the MI equation (K\*U\*Th) corresponds to the multiplication of the channels of the gamma spectrometric data. The MI helps delineate domains with higher or lower magnetism without the influence of the most superficial portions represented by soils and/or overlying duricrusts rich in iron.

$$ASA = \sqrt{dx^2 + dy^2 + dz^2}, \quad (3)$$

where ASA is the amplitude, dx and dy are the horizontal derivatives and dz is the vertical derivative.

The final products of the LI and the MI are presented in maps where favorable areas for the occurrence of lateritic duricrusts are highlighted (LI) with the different magnetic domains (MI) (Figures 9 and 10).

### 3.2. Regolith Geochemistry

Samples were collected and used for the regolith geochemistry studies, among them 586 samples of stream sediments collected in the main drainage channel with a nylon sieve (1 mm), 428 soil samples collected priorizing horizon B, and 35 samples of lateritic duricrusts. The stream sediments samples were collected from an area of about 11,550 km<sup>2</sup>, which resulted in approximately one sample per 19 km<sup>2</sup>, an appropriate density for the scale of the study, while soil samples were collected in a regular grid with a 4-km spacing. The stream sediments and soil samples were sieved at 80 mesh (1 mm), pulverized, and digested with aqua regia to analyze 54 elements by Inductively Coupled Plasma-Optical Emission Spectrometry and ICP-MS (Inductively Coupled Plasma-Mass Spectrometry; Ag, Al, As, Au, B, Ba, Be, Bi, Ca, Cd, Ce, Co, Cu, Cr, Cs, Fe, Ga, Ge, Hf, Hg, In, K, La, Li, Lu, Mg, Mn, Mo, Na, Nb, Ni, P, Pb, Rb, Re, S, Sb, Sc, Se, Sn, Sr, Ta, Tb, Te, Th, Ti, Tl, U, V, W, Y, Yb, Zn, and Zr). The lateritic duricrusts samples were crushed and pulverized in a puck mill, and the same trace elements of the stream sediments and soil geochemistry (except for Hg, B, and Re) and REEs (rare earth elements) were analyzed. In all the samples, the 54 trace elements were analyzed by both Inductively Coupled Plasma-Optical Emission Spectrometry and ICP-MS, while REE were analyzed by ICP-MS only. The major oxides in the lateritic duricrust (Al<sub>2</sub>O<sub>3</sub>, Fe<sub>2</sub>O<sub>3</sub>, SiO<sub>2</sub>, CaO, K<sub>2</sub>O, Na<sub>2</sub>O, MgO, TiO<sub>2</sub>, and P<sub>2</sub>O<sub>5</sub>) were analyzed by X-ray fluorescence after lithium metaborate and tetraborate fusion (fused beads). The preparation of the samples was performed in the Mineral Analysis Laboratory of the Brazilian Geological Survey and the chemical analyses in the SGS Geosol Laboratory LTDA, Brazil.

The data were analyzed through univariate statistics (summary of estimators, histograms, and plots of normal probability) and multivariate statistics (correlation matrix and principal component analysis, PCA) and interpreted with the support of the geological base. The samples with more than 30% of the chemical analysis below the detection limit were discarded, and those with sporadic results below the detection limit were multiplied by 0.5, according to Reimann et al. (2008). In the correlation matrix, the intervals (*r*) used (*weak to perfect*) were the same as mentioned in section 3.1. In the PCA the elements with correlations above 0.60 were used. In the selection of the factors, eigenvalues higher than 1 were used (Cattell, 1966), and to maximize the variance, the varimax rotation was used (Kaiser, 1958). These values were selected because they can explain



significant part of the variance of the data that was later correlated with the main geological features of the area. The scores of the samples, as defined for each factor, were interpolated by the inverse of the distance and used in the preparation of the geochemical maps (anomalous zones) of stream sediments and soil.

### 3.3. Regolith Mapping

The procedure to map the regolith used field descriptions of 875 sites, including those studied for this paper and others from the CPRM database (Geosgb, CPRM - Serviço Geológico do Brasil, 2016), the analysis of geomorphological and geological characteristics of the area, and the interpretation of WII, LI, and altimetry (SRTM) data, as well as geochemical data. These data were associated with the genetic model of Anand et al. (1993) that subdivides the regolith into three main regime classes: residual (relict), erosional, and depositional.

The description of the sites was conducted considering pedological aspects, including color, texture, structure (such as columnar in lateritic duricrusts), and granulometry. Regarding the geomorphology, the main landforms were evaluated together with the associated regolithic materials (Anand & Paine, 2002; Craig, 2001). These data were also evaluated in the context of the altimetry (SRTM) that is fundamental data for the definition of the occurrence mode of lateritic duricrust (residual laterites), since they occur on flat surfaces with angles less than 5° and on altitudes below 300 m and above 500 m. The geological data helped to delimit the bedrock and textural, structural, and mineralogical aspects.

To delimit the boundaries of the regolithic units, in addition to field data, aero geophysical data were used, including gamma-spectrometric data and associated indexes (WII and LI). The gamma-spectrometric patterns (Th, U, K, and ratios of Th/K and U/K) were correlated with the respective weathering intensity to support the regolith cartography.

The geochemical associations were used to evaluate the regolith response patterns, for example, geochemical associations of alkali and earth-alkali elements are related to rocky outcrops and/or saprolite; on the other hand, associations with Al and Ga are related to the presence of residual units. The geochemical associations were also compared with the gamma-spectrometric results (WII and LI), which contributed to the refinement of the cartography of the main regolithic units, as proposed by Craig (2001), in addition to giving support to the evaluation and identification of eventual false anomalies. All of the mentioned bases were integrated and analyzed as information layers to map and characterize the different regolithic units. In this sense, each data set was used to add a different component of information to the final product (the regolith map).

The materials that constituted the main regolithic units described and represented in the regolith map include rocky outcrops, coarse and fine saprolite, soil, lateritic duricrusts, and transported sediments (Figure 11). The lateritic duricrusts in the area do not show evidence of transportation, and therefore, it is important to highlight that the area mainly consists of residual material (in situ).

In the regolith map, the units were divided into in situ regolith and transported regolith. In situ regolith was subdivided into pedolith, in which soils and lateritic duricrusts are predominant (residual) and saprolite, in which saprolite and saprock are predominant (erosional). Alluvial deposits were included in the transported regolith (depositional), while rocky outcrops were described as bedrock on the map. The flowchart in Figure 2 shows the products used in the indexes: the WII (black arrow), LI (red arrows), MI (blue arrows), and the regolith map, as well as the integration with the geochemistry and geophysics, which led to the final interpretations and discussions (yellow arrows).

## 4. Results and Discussions

### 4.1. Geochemistry

#### 4.1.1. Stream Sediments

In the stream sediment analysis of all elements mentioned in section 3.3, measurements of Ag, As, Au, B, Ge, Hg, S, Sb, Re, Se, Ta, Te, and W have 30% or more of the samples below the detection limit and, therefore, were not used in the statistical calculations.

Univariate statistics identified 41 anomalous elements when compared to the regional background (Al, Ba, Be, Bi, Ca, Cd, Ce, Co, Cr, Cs, Cu, Fe, Ga, Hf, In, K, La, Li, Lu, Mg, Mn, Mo, Na, Nb, Ni, P, Pb, Rb, Sc, Sn, Sr, Tb, Th, Ti, Tl, U, V, Y, Yb, Zn, and Zr) and 149 anomalous sites that delimited three anomalous zones (I, II, and III)

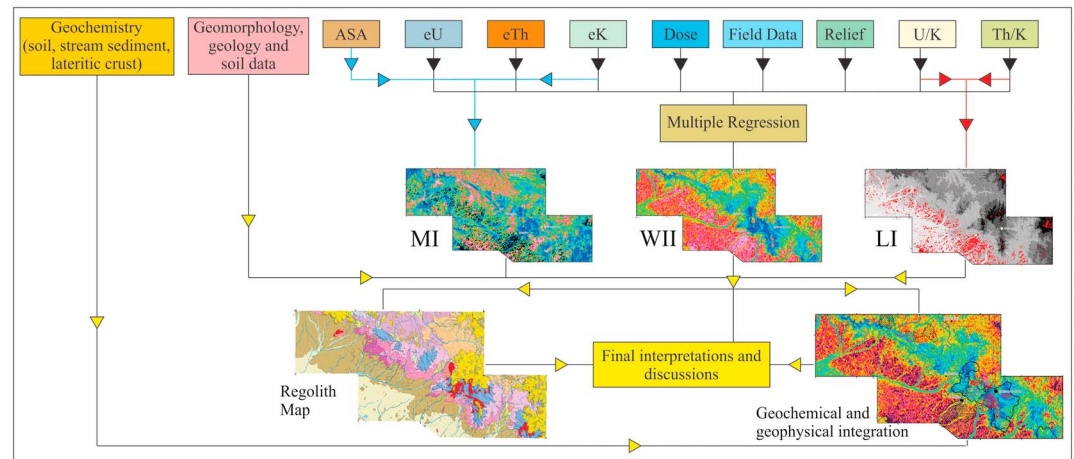


**Figure 2.** Summary of procedures for mapping the regolith and lateritic duricrusts and then integrating the geochemical and geophysical data. ASA = analytic signal amplitude; WII = weathering intensity index; MI mafic index; LI = lateritic index.

represented by two or more contiguous watersheds (Figure 3). The anomalous Zone I, defined by the association of Cu-Fe-Ni-V, covers 135 km<sup>2</sup> on the northeast side of the area and consists of watersheds draining basalts, diabbases, gabbros, conglomerates, sandstones, siltstones, and claystones. The anomalous Zone II, defined by the association of Al-Co-Cu-Cr-Fe-Ga-Ni-Sc-V, covers 158 km<sup>2</sup> in the central-north region of the study area and corresponds to watersheds draining basalts, diabbases, and gabbros. The anomalous Zone III, defined by the association of Ce-Hf-La-Nb-P-Tb-Th-U-Y-Yb-Zr, covers 628 km<sup>2</sup> in the central-southwest region of the area and corresponds to watersheds draining granitoids, supracrustals, sandstones, and associated lateritic duricrusts. In other regions of the study area, there are isolated anomalies, highlighting Cd-Zn, Ca-Mg-Na, Bi-Tl, Be-Cs-K-Li-Rb-Tl, Al-Ga, and Bi-Cd-Tl, or single anomalies of Bi, Ca, Cd, Co, Cr, Cs, Cu, Hf, In, La, Ni, Pb, Sr, Ti, Tl, U, and V.

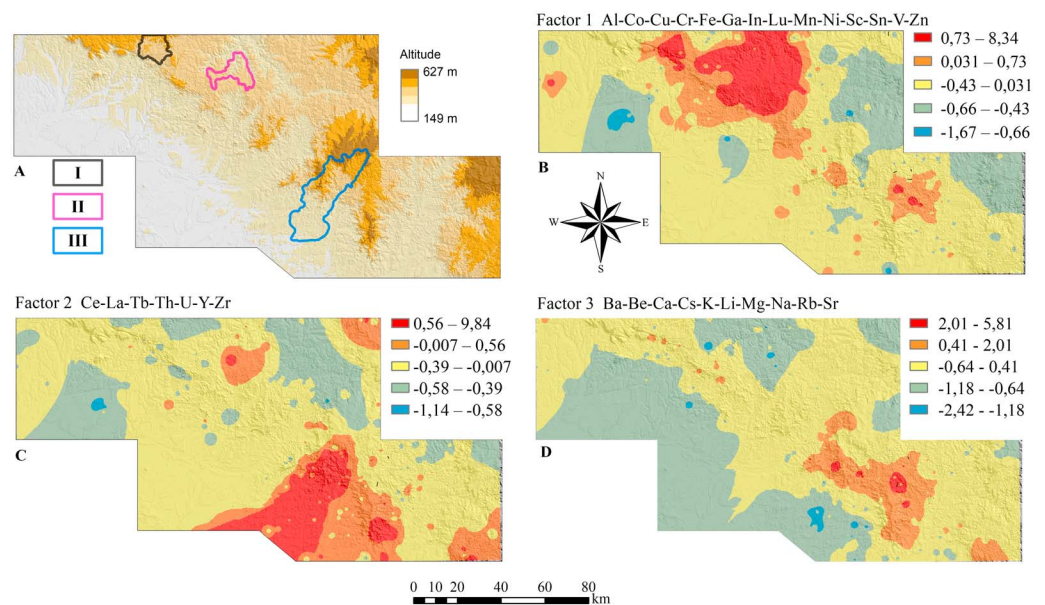


**Figure 3.** (a) Anomalous Zones I, II, and III represented by two or more contiguous watersheds. (b–d) Maps of stream sediment geochemical zones (interpolated scores, high-score regions above the regional background are shown in red and orange).

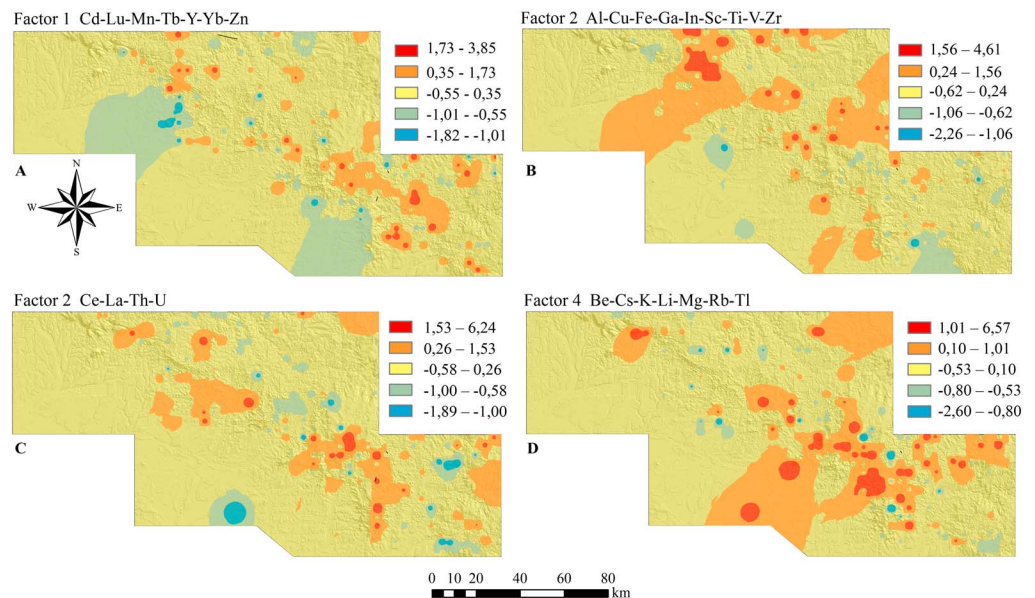


**Figure 4.** Maps of anomalous soil geochemical zones (interpolated scores, high-score regions above the regional background in red and orange) integrated with the relief.

The PCA showed that the three main factors account for 74.13% of the variance. Factor 1 (Al-Co-Cr-Cu-Fe-Ga-In-Lu-Mn-Ni-Sc-Sn-V-Zn) corresponds to 44.69% of the variance and is associated with basalts, diabases, gabbros, and subordinately schists and paragneisses. Factor 2 (Ce-La-Tb-Th-U-Y-Zr) accounts for 17.18% of the variance and is related to granitoids and associated lateritic duricrusts, supracrustal rocks, and sandstones. Factor 3 (Ba-Be-Ca-Cs-K-Li-Mg-Na-Rb-Sr) corresponds to 12.26% of the variance and is related to supracrustal rocks and its saprolites, located in the IZ and LPS (Figure 3). The other factors have low variance (<5%) and have no geological meaning.

#### 4.1.2. Soil

Among the elements analyzed in the soil samples, V (689 ppm), Cr (717 ppm), Cu (516 ppm), Ni (312 ppm), Ce (280 ppm), La (111 ppm), and Y (125 ppm) showed the highest concentrations, but the concentrations are within the averages found in the Earth's crust, rocks, and/or weathered products (Wedepohl, 1969). Silver, Au, As, B, Ge, Hf, Hg, Na, Re, Se, Ta, Te, and W are below the detection limit in at least 30% of the samples and were discarded. The PCA highlighted four factors that account for 69.71% of the variance. Factor 1, defined by the association of Cd-Lu-Mn-Tb-Y-Yb-Zn, and corresponding to 34.53% of the total variance, is related mainly to the paragneisses and schists located in the IZ and, locally, to the sandstones of the UPS. The association of Al-Cu-Fe-Ga-In-Sc-Ti-V-Zr defined factor 2, which accounts for 18.83% of the variance and is associated with a large part of the IZ and UPS in the northwest and central part of the area, where there are basalts, diabases, and gabbros, in addition to sandstones and siltstones. Factor 3, defined by the association of Ce-La-Th-U and corresponding to 10.51% of the variance, is related to the granitoids and lateritic duricrusts over the LPS and, subordinately, over the sandstones in the IZ and the UPS. Factor 4, defined by the association of Be-Cs-K-Li-Mg-Rb-Tl and accounting for 5.84% of the variance, is related to the granites, gneisses, para-derived rocks, and their saprolites located in the IZ, the UPS, and subordinately on the LPS (Figure 4).

#### 4.1.3. Lateritic Duricrusts

The samples of the LPS have an inverse relationship between  $\text{Fe}_2\text{O}_3$  and  $\text{SiO}_2$  ( $\text{Fe}_2\text{O}_3/\text{SiO}_2$  average of 1.36), while  $\text{Al}_2\text{O}_3$  shows no relationship with  $\text{SiO}_2$  (dispersion), presenting an  $\text{Al}_2\text{O}_3/\text{SiO}_2$  average of 0.53 (Figure 5a).  $\text{TiO}_2$ ,  $\text{K}_2\text{O}$ ,  $\text{P}_2\text{O}_5$ ,  $\text{CaO}$ ,  $\text{MgO}$ , and  $\text{Na}_2\text{O}$  have contents below 2% (supporting information), and the correlation with major oxides shows dispersion. Among the trace elements, Ba, Cd, Cr, Cs, K, Ni, P, Pb, Rb, Sr, Ta, and V are above the regional background in 17 sites. Of those, only Ta (10.47 ppm) and V (2723 ppm) are 3 to 5 times above the average concentration of lateritic duricrusts (Hill et al., 2001; Kotschoubey et al., 2005; Tardy, 1993; Wedepohl, 1969) indicating relevant anomalies. REEs have an average of 72.9 ppm; there is an enrichment of light REEs (LREEs) relative to heavy REEs (HREEs) ( $\text{LaN/YbN} = 3.22$ ), and



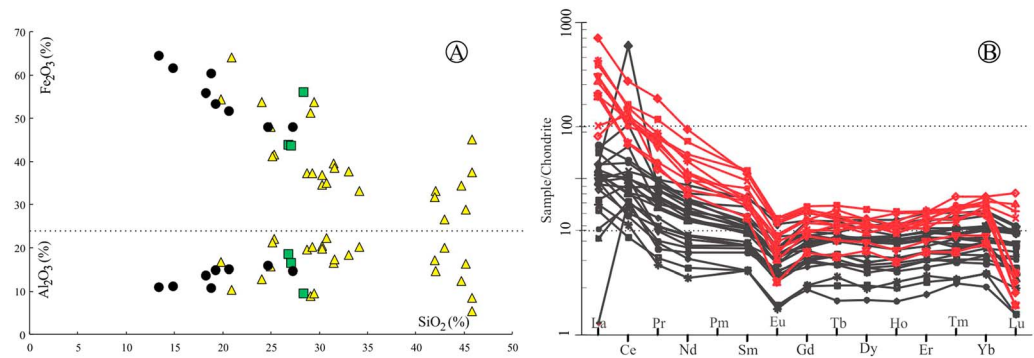


**Figure 5.** (a) Fe<sub>2</sub>O<sub>3</sub> versus SiO<sub>2</sub> (top) and Al<sub>2</sub>O<sub>3</sub> versus SiO<sub>2</sub> (bottom). ● UPS; ■ IZ; ▲ LPS. (b) Chondrite-normalized REE plots (Taylor and MacLennan, 1985), LPS (black), UPS + IZ (red). REE = rare earth element; LPS = lower planation surface; IZ = intermediate zone; UPS = upper planation surface.

the average of Eu/Eu\* and Ce/Ce\* anomalies are 0.64 and 2.75, respectively (Figure 5b, supporting information). The plot of Al<sub>2</sub>O<sub>3</sub> – Fe<sub>2</sub>O<sub>3</sub> – (CaO + K<sub>2</sub>O + MgO + Na<sub>2</sub>O + P<sub>2</sub>O<sub>5</sub>) highlights samples with higher alkali values and less iron content when compared to the samples of the UPS and the IZ (Figure 6b). These samples are classified as laterite and subordinately as ferruginous and fersiallitic laterites, which is related to moderate lateritization (Dury, 1969; Schellman, 1981; Schellmann, 1983, Figures 6a and 6c).

Similar to the LPS, the samples of the UPS have an inverse relationship between Fe<sub>2</sub>O<sub>3</sub> and SiO<sub>2</sub> (Figure 5a); however, the average ratio is higher at 3.01. Al<sub>2</sub>O<sub>3</sub> and SiO<sub>2</sub> are directly proportional (Figure 5a) and have an average ratio higher than the LPS (average of 0.7). TiO<sub>2</sub>, K<sub>2</sub>O, P<sub>2</sub>O<sub>5</sub>, CaO, MgO, and Na<sub>2</sub>O have concentrations lower than those found in the LPS, except for P<sub>2</sub>O<sub>5</sub>, and show a dispersion pattern when correlated individually to major oxides. Among the trace elements, only Ta and V have concentrations above average lateritic duricrusts and bauxites (11.29 and 1,849 ppm, respectively, Hill et al., 2001; Kotschoubey et al., 2005; Tardy, 1993; Wedepohl, 1969). REEs have an average concentration of 52.4 ppm, with strong enrichment of the LREEs (LaN/YbN = 6.61) and ratios Eu/Eu\* and Ce/Ce\* of 0.64, which is generally lower than those found in the LPS (Figure 5b), while the ratio LaN/YbN is approximately 2 times higher. In general, there is a lower concentration of Co + Cr + Ni and a higher Th/K ratio when compared to the LPS (Figures 6d and 6e). The plot of Al<sub>2</sub>O<sub>3</sub> – Fe<sub>2</sub>O<sub>3</sub> – (CaO + K<sub>2</sub>O + MgO + Na<sub>2</sub>O + P<sub>2</sub>O<sub>5</sub>) highlights the high content of Fe<sub>2</sub>O<sub>3</sub> and simultaneously low content of alkali in the UPS (Figure 6b). These samples are classified as ferruginous and fersiallitic laterites and are related to intense lateritization (Dury, 1969; Schellman, 1981, 1983, Figures 6a and 6c).

The samples of the IZ have Fe<sub>2</sub>O<sub>3</sub> and alkali concentrations similar to those on the UPS, including high values of Fe<sub>2</sub>O<sub>3</sub> and simultaneously low values of alkali (Figure 6b). The average Fe<sub>2</sub>O<sub>3</sub>/SiO<sub>2</sub> ratio is 1.74, while the average Al<sub>2</sub>O<sub>3</sub>/SiO<sub>2</sub> ratio is 0.54. TiO<sub>2</sub>, K<sub>2</sub>O, P<sub>2</sub>O<sub>5</sub>, CaO, MgO, and Na<sub>2</sub>O have lower contents than those on the LPS. None of the trace elements are above the regional background. REEs have an average concentration of 43 ppm, average Eu/Eu\* of 0.56, LaN/YbN ratio of 4.3, and Ce/Ce\* of 0.90. The REEs concentrations and the Eu/Eu\* and Ce/Ce\* ratios are lower than those on the other surfaces, but the LaN/YbN ratio is higher than on the LPS. The Th/K – U/K – SiO<sub>2</sub>/Fe<sub>2</sub>O<sub>3</sub> and REE – CoCrNi – ScYzr plots are similar to the UPS, as are the high Th and low K and U concentrations (Figures 6d and 6e). These samples are classified as laterite/ferruginous and fersiallitic laterite and are related to moderate lateritization (Figures 6a and 6c).

The PCA identified six factors that account for 81.6% of the variance and define the following geochemical associations: REE-(La + Ce) (factor 1), In-La-Mo-Sn-Ta-Te-W (factor 2), Cs-Ge-K-Ni-Rb-Sr-Y (factor 3), Hf-Th-Zr (factor 4), Cu-Sc-U (factor 5), and Ba-Ce-Nb-Pb (factor 6), primarily associated with residual minerals (including zircon, monazite, and muscovite).

The weathering indexes CIA (Chemical Index of Alteration) and WIP (Weathering Index of Parker) (Nesbitt & Young, 1982 and Parker, 1970, respectively) indicate that the lateritic duricrust samples have weathering rates similar to those from Africa, Guyana, and India (Giorgis et al., 2014; Harrison, 1934; Wimpenny et al., 2007) (Figure 7) and significantly higher than those from Iran, Ireland, China, and Australia (Asghar Calagari et al., 2015; Cornelius et al., 2007; Hill et al., 2000; Xiao et al., 2014).

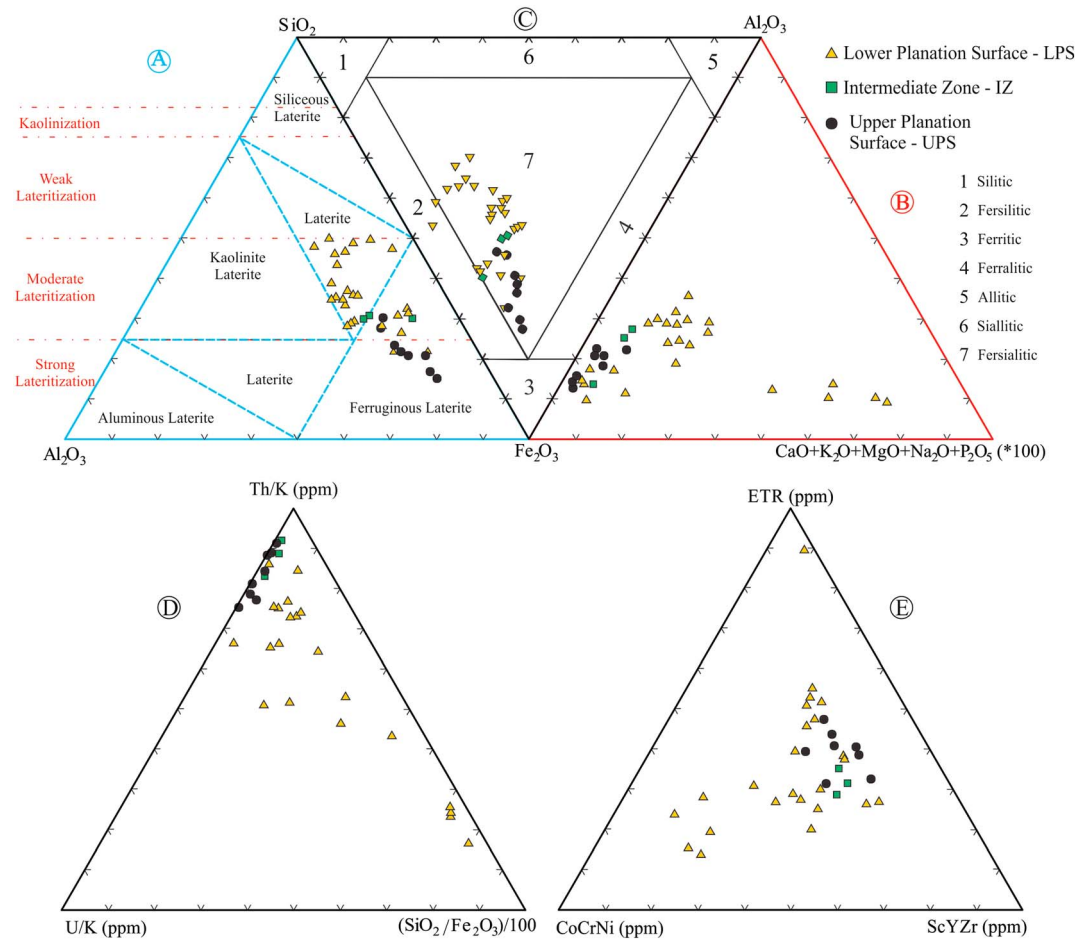


**Figure 6.** (a) Ternary plot of SiO<sub>2</sub> – Al<sub>2</sub>O<sub>3</sub> – Fe<sub>2</sub>O<sub>3</sub> (Schellmann, 1983) and degree of lateritization. (b) Ternary plot of Al<sub>2</sub>O<sub>3</sub> – Fe<sub>2</sub>O<sub>3</sub> – alkali showing the decrease of alkali on the UPS. (c) Ternary plot of SiO<sub>2</sub> – Fe<sub>2</sub>O<sub>3</sub> – Al<sub>2</sub>O<sub>3</sub> (Dury, 1969) highlighting the fersiallitic classification of most of the samples. (d) Ternary plot of Th/K – U/K – SiO<sub>2</sub>/Fe<sub>2</sub>O<sub>3</sub>/100 that shows higher values of Th and Fe<sub>2</sub>O<sub>3</sub> and lower values of K in the samples of the UPS. (e) Ternary plot of REE – CoCrNi – ScYZr showing the samples of the LPS with high values of CoCrNi and low values of REE and lower values of CoCrNi and high values of REE on lateritic duricrusts derived from sandstones.

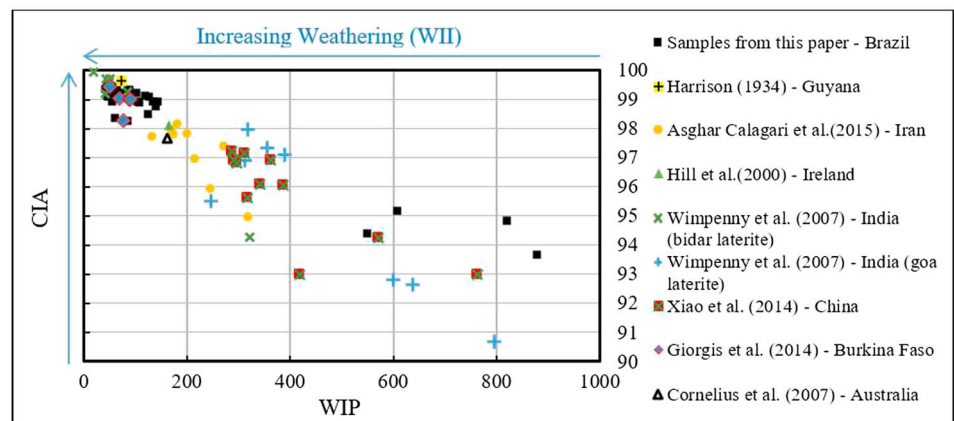


**Figure 7.** Plot of WIP versus CIA of lateritic duricrusts of the study area and other parts of the world.

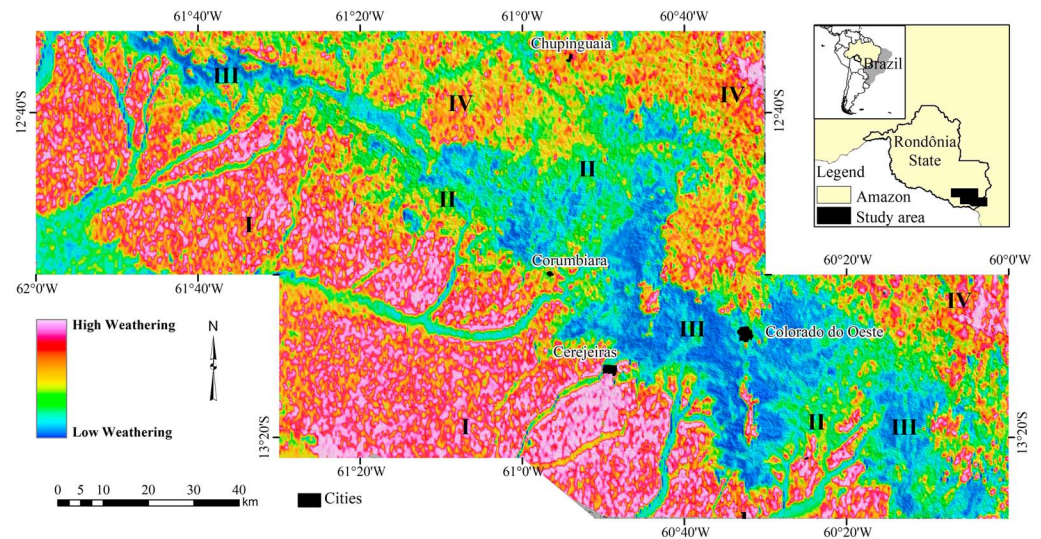


**Figure 8.** Weathering intensity index (WII) overlying the shaded altimetry highlighting the main domains of weathering.

#### 4.2. Weathering Intensity Index

The classification of the weathering level allowed the distinction of areas with similar weathering characteristics (Table 1). The WII highlighted four major domains: (i) the south-southwest-west side of the area (altitudes below 300 m), mainly distinguished by the high weathering intensity (WCs = 4 and 5; red in Figure 8) that corresponds to alluvial deposits, lateritic duricrusts, dismantling products, and oxisols; (ii) the southeast-central-northwest region (altitudes between 300 and 500 m) marked by intermediate weathering intensity (WC = 3; green and yellow in Figure 8) that corresponds to the sites with weathered rocky outcrops (saprolite); (iii) the southeast-central-northwest areas (altitudes between 300 and 500 m) with low weathering intensity (WCs = 1 and 2, blue in Figure 8) and mafic rock outcrops, schists, and granites with weak or no weathering at all; and (iv) the north and northeast regions (altitudes above 500 m) with a high weathering intensity (WCs = 4 and 5; red and pink in Figure 8) and the presence of lateritic duricrusts and oxisols. Both domains *i* and *iv* are partially coincident with the areas predicted as favorable for the occurrence of lateritic duricrusts and oxisols in Iza et al. (2016).

#### 4.3. Lateritic Index

The calculation of the LI highlighted four major domains: (i) the south-southwest-west regions of the area (altitudes below 300 m) mainly marked by a high LI (red to pink in Figure 9); (ii) the southeast-central-northwest portions of the area with altitudes between 300 and 500 m with an intermediate LI (green and yellow in Figure 9); (iii) the southeast-central-northwest regions of the area associated with altitudes between 300 and 500 m and with a low LI (blue in Figure 9); and (iv) north and northeast regions of the area with altitudes above 500 m, with a high LI (red to pink in Figure 9). Overall, the domains previously described cover the same geological domains as the WII. The main differences between the WII and the LI are in the *i* and *iii* domains where there are areas that are slightly more weathered (more continuous) on the WII than on the LI.

The predicted areas for the occurrence of lateritic duricrusts that are defined by the LI and WII represent approximately 7.5% and 8% of the area, respectively. These values are lower than those found by Iza et al. (2016) using fuzzy gamma operator 0.7, which found approximately 11% of the area with the potential for the occurrence of lateritic duricrusts. These areas have a strong relationship with flat areas (slopes <5%) and with altimetry below 300 m and above 500 m. This disparity is probably associated with the methods and mathematical techniques used in the corresponding models. In any case, these areas (domains *i* and *iii*) are considered to have higher probability of occurrence of lateritic duricrusts and therefore related to the dominance of residual processes.



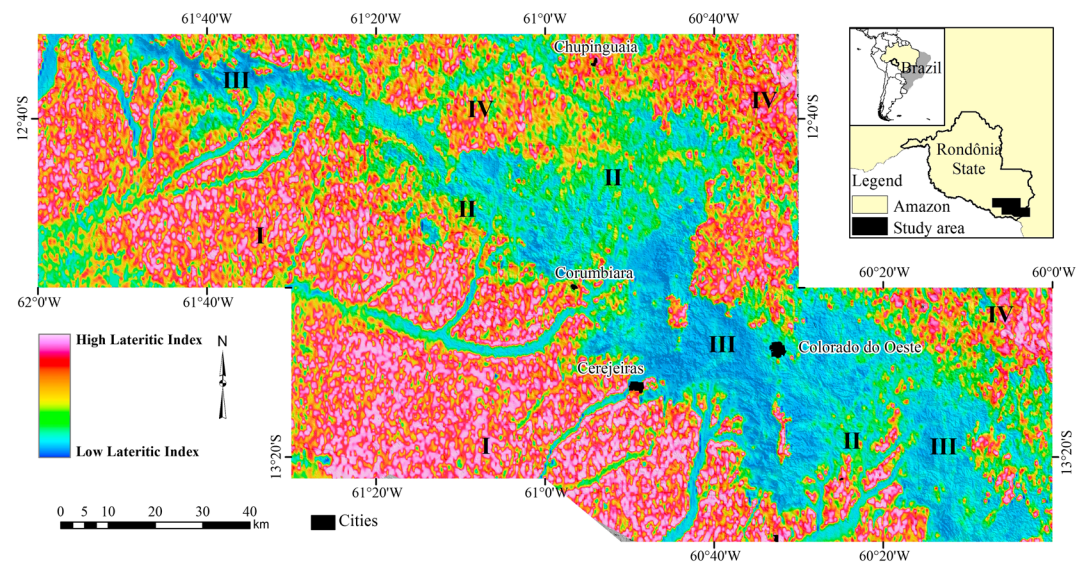


**Figure 9.** Lateritic index (LI) overlying the shaded altimetry highlighting the main domains.

#### 4.4. Mafic Index

The MI defined four major domains according to the magnetic degree: (i) the north side with a dominantly magnetic substrate, associated mainly with mafic rocks (red to pink in Figure 10); (ii) the central-southeast and southeast side of the area of less magnetic materials associated with granitoid rocks (blue in Figure 10); (iii) the northwest-central-south region (LPS), where there is an alternation of magnetic materials with less magnetic materials related to para-derived rocks, gneisses, and granitoids. (blue and pink in Figure 10); and (iv) the northeast-central region, where there is an alternation of magnetic materials with less magnetic materials that is related to the Parecis Basin that consists of sandstones and siltstones (blue and pink in Figure 10). The areas with high LI (more intensely lateritized, represented by the areas with the average LI plus 1.5 times the standard deviation) overlap on the northeast side with domains that are less magnetic (sandstones) and overlap on the northwest and south region with domains that have both high

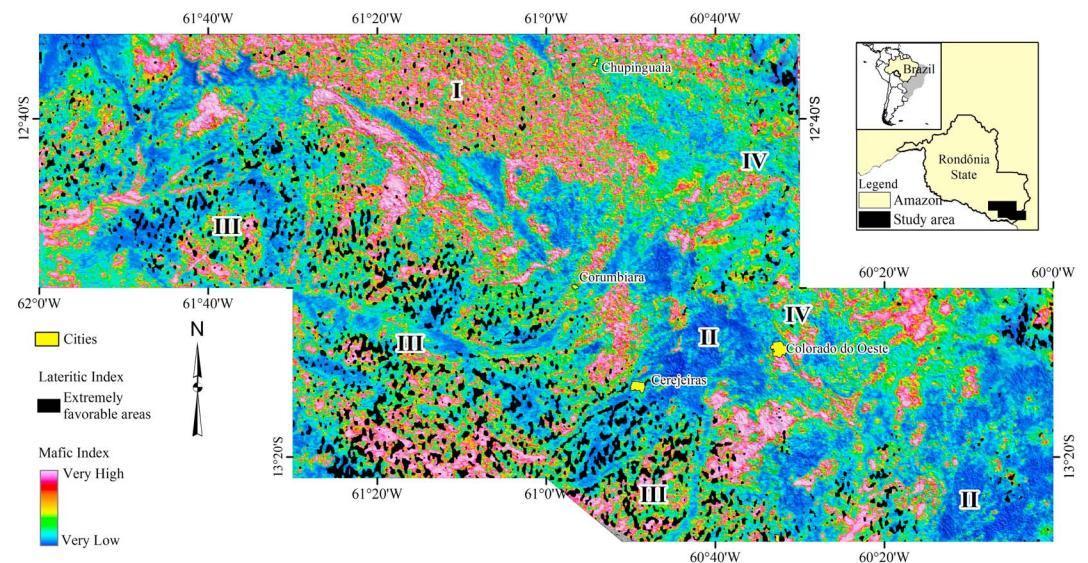


**Figure 10.** Lateritic index (high values in black) overlying the mafic index (MI) highlighting the four main domains.



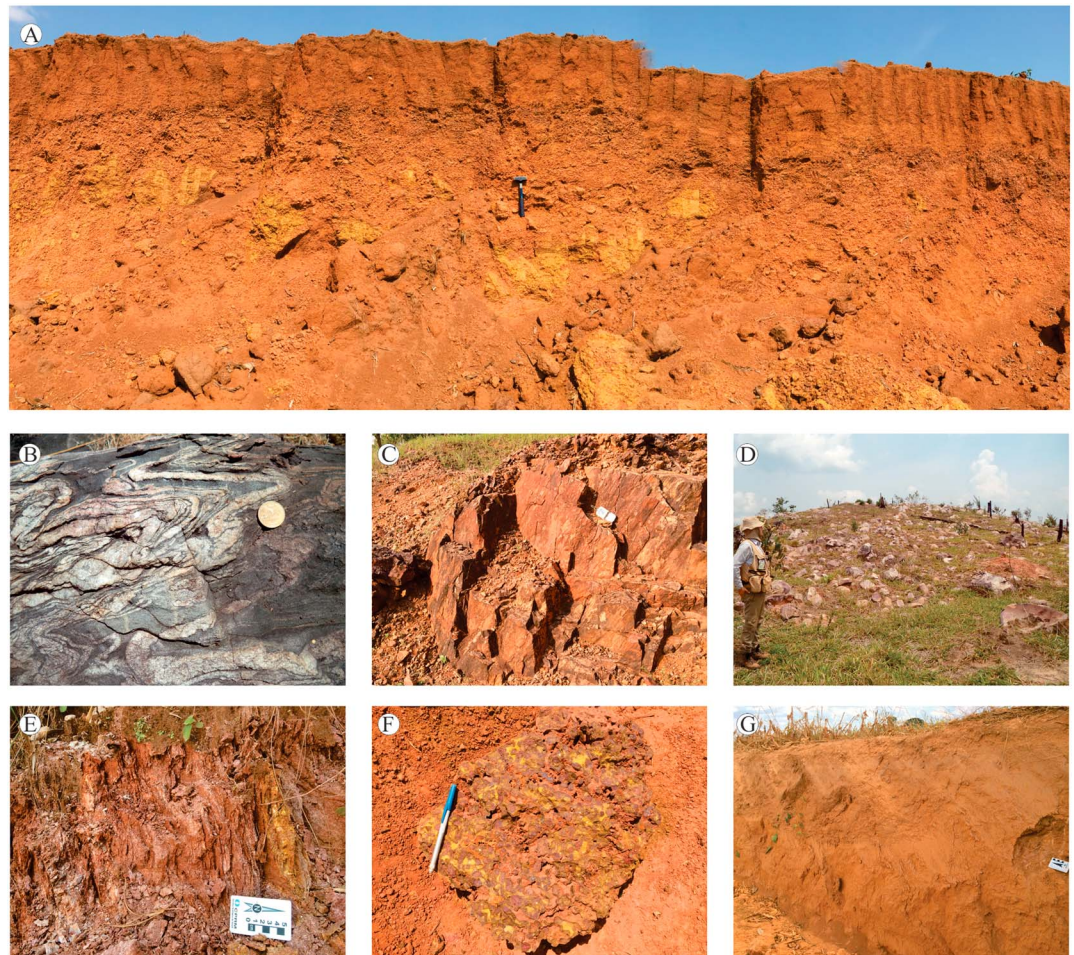


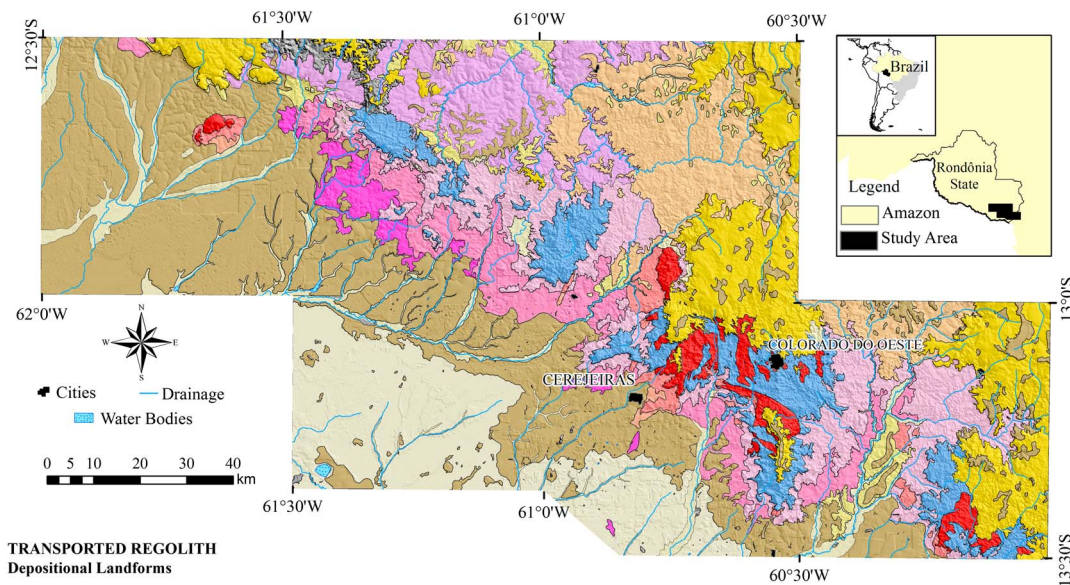
**Figure 11.** (a) Ferruginous lateritic duricrust. (b–d) Bedrock and respective outcrops. (e) Schist saprolite. (f) Pisolithic/nodular lateritic duricrust boulder. (g) Oxisol.

and low MI (mafic and felsic rocks, respectively, Figure 10). These results are important to clarify the origin of the lateritic duricrusts (parental rocks), especially those located on the LPS (iii, northwest-south), where the quantity of rocky outcrops is limited and the area is mainly covered by soils and sediments.

#### 4.5. Regolith Map

The integration of multisource data is allowed for the delimitation of the regolithic units and, therefore, domains with higher or lower weathering intensity. The aero geophysical data highlighted domains with high ratios of Th/K and U/K, which were in some cases overlaid by geochemical associations related to residual processes, such as Al-Fe-Ga-V and Ce-La-Tb-Th-U. On the other hand, the geophysical domains interpreted to have low weathering intensity (low ratios eTh/K and eU/K) and areas with low LI overlapped well with the geochemical associations that had a predominance of alkaline and alkaline-earth elements. These results related to altimetry, geomorphology, and field work allowed the delimitation of the units shown on the regolith map (Figure 12). The field data helped to confirm the interpretations that were made beforehand. Figure 11 shows some of the main regolithic materials mapped, together with the bedrock. It is important to highlight that in the Amazon region and in several parts of Brazil, often the residual domains and sedimentary units are mapped as a single unit called *undifferentiated sedimentary cover* or *detritus-lateritic cover*.

In this context, the area mapped as undifferentiated sedimentary cover (Quadros et al., 2007) was interpreted and mapped as residual material because it represents oxisols, lateritic duricrusts, and dismantling products. Therefore, the regolith map (Figure 12), which is a first of its kind in the Amazon, was developed based on



**TRANSPORTED REGOLITH**  
**Depositional Landforms**

Alluvial deposits consisting mostly of sand, gravel, clay and silt, mainly associated with the flood plain of the Guaporé river tributaries and subject to periodic floods. The relief is plain and related to fluvial plains and terraces with altitudes below 300 m. On altitudes below 250 m swampy terrains consisting of clay and silt may occur.

**IN SITU REGOLITH**

**Pedolith**

- Lateritic crusts and dismantling products besides oxisols, associated with plain relief occurring mainly in altitudes below 300 m and above 500 m.
- Quartzipsamment and coarse saprolite derived from sandstones, arcosean sandstones and siltstones. The landforms have flat tops and altitudes between 300 and 500 m.
- Red to yellow dystrophic ultisols with rare occurrence of coarse and fine saprolite, basalts, diabases and gabbros located on altitudes below 400 m. The relief has tabular and convex tops.
- Red-yellow eutrophic ultisol with frequent occurrence of coarse and fine saprolite derived from granitic rocks, located on altitudes of up to 400 m. The landforms have convex tops and sometimes evidence structural control.
- Red-yellow eutrophic ultisol with eventual occurrences of fine saprolite derived from granitic rocks, located on altitudes of up to 300 m.
- Red-yellow dystrophic ultisol with medium to fine texture mainly associated to paraderived rocks. Outcrops of fine saprolite are rares and altitudes reach 300 m.

**Saprolith**

- Fine saprolite, clayey horizon and colluvium derived from paraderived rocks. The relief is plain with eventual convex tops, with maximum altitudes of 350 m.
- Sandstones, arcosean sandstones and siltstones commonly associated with coarse saprolite to quartzipsamment. The landforms have flat tops and altitudes are below 500 m.
- Coarse and fine saprolite, consisting of basalts, diabases and gabbros located on altitudes below 400 m. The occurrence of red-yellow dystrophic ultisols is common. The relief has tabular and convex tops.
- Coarse saprolite, and colluvium locally derived from paraderived rocks. The landforms have convex tops and, in general, evidence structural control. The altitudes vary between 350 and 500 m. The soils are mainly ultisols and subordinately alfisols.

**Bedrock**

- Sandstones, arcosean sandstones and siltstones with eventual coarse saprolite. The landforms have flat tops and are rarely convex. The altitudes are above 500 m.
- Granitic rocks sometimes with little signs of decomposition and eventual occurrence of coarse saprolite, located on altituded of up to 400 m. The landforms have convex tops and sometimes evidence structural control.
- Paraderived rocks with very rare presence of coarse saprolite. The landforms have convex tops and, in general, evidence structural control. Altitudes vary between 350 and 500 m.

Figure 12. Regolith map.

fieldwork and supported by the WII, LI, and the results of Iza et al. (2016). This integration showed an expansion of the areas more intensely weathered and strongly related to residual materials (Figures 1 and 11). It was confirmed that the highly weathered domains (Figures 8 and 9) are associated with lateritic duricrusts and oxisols on the UPS and on the LPS, as indicated by Iza et al. (2016).

## 5. Integration of Geochemical and Geophysical Data

The study of regolith using gamma ray spectrometric data has been discussed by several authors (e.g., Barbosa et al., 2013; Carrino et al., 2011; Dauth, 1997; Herrera et al., 2017; Iza et al., 2016; Wilford, 2012). They remark that high Th/K and U/K ratios (in this paper between 254 and 1148 and between 29 and 111, respectively) have an excellent correlation with lateritic duricrusts.



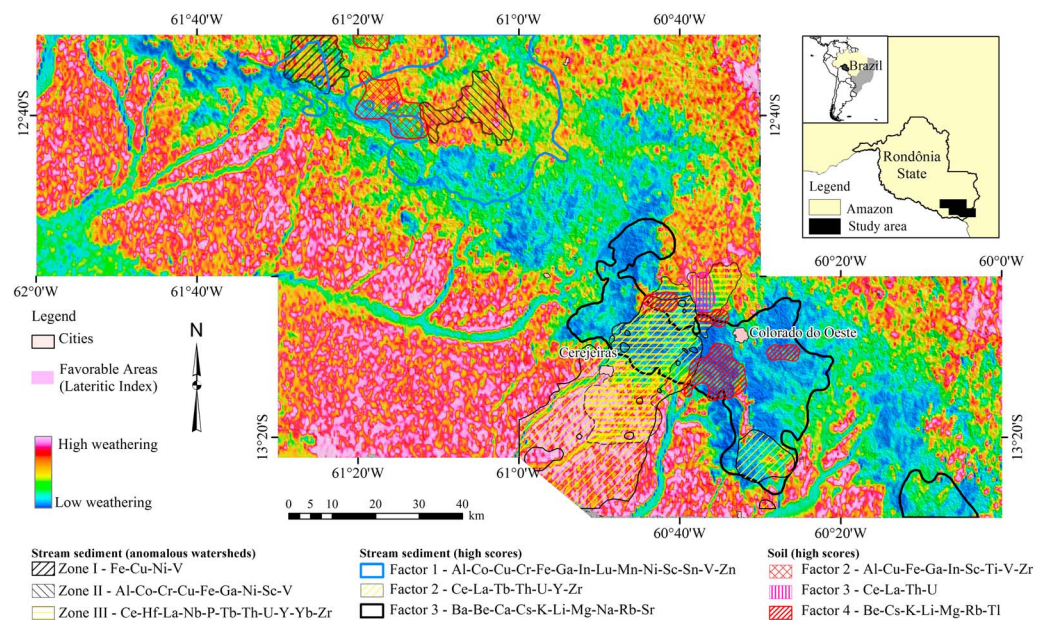


**Figure 13.** Map of WII, with anomalous watersheds, highest scores of geochemical associations (from the stream sediments and soil), and the areas with a high probability of occurrence of lateritic duricrusts (as defined by the lateritic index, LI). WII = weathering intensity index.

On the other hand, it is important to highlight that during the weathering process, elements such as Al, Fe, Ga, Th, U tend to be enriched in the lateritic profile, while elements such as Ca, Na, K, and Mg are leached, causing a strong concentration decrease.

With this in mind, the gamma spectrometry, more specifically, WII and LI, contributed to the mapping of regolith that was previously considered sedimentary by other authors (for example, in the identification of lateritic domains; residual). This reinterpretation can be extrapolated to the entire western region of the Brazilian Amazon, thereby expanding the areas with mineral potential related to supergene enrichment. The WII and LI also contributed to the indication of areas with lower weathering indexes and, thus, with higher probabilities of rocky outcrops occurrences. These results supported the interpretations about the superficial processes and the regolith map. On the other hand, the geochemical results presented in this study helped to understand the weathering process of the area because they discriminated between domains with geochemical associations strongly related to high and low weathering.

The correlation, for example, between WIP and CIA reflects the high weathering indexes in the Amazon relative to those in China, India, Iran, Ireland, and Australia (Figure 7). Additionally, the WII, as well as the LI, has excellent spatial correlation with geochemical data from soil and stream sediments. The high concentrations of Al, Ce, Co, Cr, Cu, Fe, Ga, Hf, Ni, Th, U, V, and Zr shown in the geochemical associations (from the soil and stream sediment geochemical results) and simultaneous lower concentrations of alkali are another geochemical criterion for the determination of highly weathered areas and the identification of lateritic domains. These results are particularly valid when compared with areas showing high WII and/or LI (Figures 8, 9, and 12). In any case, the WII is shown to be more robust because it considers the altimetry and delimits weathering areas (high and low) and considers more than just the domains with a higher probability of lateritic duricrusts occurrence.

The MI, supported by the geochemical results of stream sediments and soil, discriminated between lateritic duricrusts developed on substrates with different magnetic signatures (mafic and felsic). The respective geochemical averages of the LPS and UPS lateritic duricrusts samples of Ba (134 and 15 ppm), Co (10 and 2.5 ppm), Cr (335 and 138 ppm), Ni (21 and 8 ppm), Rb (12 and 2 ppm), and Th (23 and 41 ppm; supporting information) support the influence of the mafic bedrock on the LPS. On the other hand, the lower concentrations of Co + Cr + Ni and simultaneous higher concentrations of Sc + Y + Zr (Figure 6e) in a set of samples reflect the felsic parent rock of those lateritic duricrusts. The stream sediments, Zones I and II,

**Table 5**  
Main Characteristics of Lateritic Duricrusts and Respective Geomorphological Domains

	Upper planation surface (UPS)	Lower planation surface (LPS) Intermediate zone (IZ)
Texture/structure	Cellular; pisolithic; nodular	Pisolithic; nodular; vermiform/columnar
Macromineralogy	+Hem; +Gt; -Kln; +Qz + Gbs	+Hem; +Gt; Kln; -Qz; -Gbs
Type of occurrence	Blocks and large outcrops	Blocks <3 m (mainly) and limited outcrops
Altimetry	Plateaus above 500 m	Floodplains below 300 m/>300 and < 500 m
Preserved fabrics (parent rock)	Not observed	Present, very rarely (schist)
Lithology	Mainly sandstones (Parecis basin)	Varied (bedrock) and recent deposits (absence of sedimentary rocks)
Geochemistry (SS) Intersection with PM <sup>a</sup>	Zone III (restrict)	Zone III/Zones I and II; Factor 1
Geochemistry (Soil) Intersection with PM <sup>a</sup>	Factor 3	Not observed
Lithogeochemical anomaly	V-Ta	V-Ta
Major elements (duricrust)	Fe <sub>2</sub> O <sub>3</sub> > SiO <sub>2</sub> (trend)	Fe <sub>2</sub> O <sub>3</sub> < SiO <sub>2</sub> (trend)
REE	LREE > HREE	LREE > HREE (Ce anomaly)
Th/K	Th » K	Th > K
Alkali (CaO, MgO, K <sub>2</sub> O, Na <sub>2</sub> O)	Lower concentration	Higher concentration
Lateritization (Schellmann, 1983)	Intense (trend)	Moderate (trend)
Classification (Dury, 1969)	Fersiallitic	Fersiallitic
WII	High index	High/low index
LI	High index	High/low index
MI	Low (predominantly)	High and low (variable)

Note. MI = mafic index; LI = lateritic index; WII = weathering intensity index; REE = rare earth element; HREE = heavy rare earth element; LREE = light rare earth element; SS = Stream Sediment.  
<sup>a</sup>PM = predictability model.

and PCA factor 1, together with soil PCA factor 2, show a good spatial overlap and delimit the weathering area of the mafic rocks, which supports part of the MI results and the high WII response.

The integration of geophysics and geochemistry, through gamma ray spectrometry, the analysis of stream sediments and soil, and the lithogeochemistry of lateritic duricrusts contributed to the regolith mapping (delineating high and low weathering boundaries) and allowed the subdivision of the study area in two major weathering domains, shown in Figure 13. Domain I is located in the central-southeast portion of the area with lower WII (WCs = 1 and 2, Table 1) and the geochemical association of Ba-Be-Ca-Cs-K-Li-Mg-Na-Rb-Sr. This domain is between 300 and 500 m high and has undulated relief and slopes between 10° and 65° corresponding to the IZ of Iza et al. (2016), where the erosive process, which exposes rocks and saprolite, is dominant over the weathering process. Domain II is located in the south-southwest-west and northeast portions of the area and has higher WII (WCs = 4 and 5, Table 1) that is related to the lateritic duricrusts and geochemical association of Al-Ce-Ga-Hf-La-Tb-Th-U-Y-Zr. In this domain, which is between 149 and 300 m and between 500 and 627 m high and mostly corresponds to the LPS and UPS of Iza et al. (2016), respectively, the weathering process is dominant over the erosive process.

The lateritic duricrusts of the UPS, where the sedimentary parent rocks are predominant, have higher Fe<sub>2</sub>O<sub>3</sub> and Th content and lower SiO<sub>2</sub> and CaO + K<sub>2</sub>O + MgO + Na<sub>2</sub>O + P<sub>2</sub>O<sub>5</sub> content. These results are allowed for the differentiation of these lateritic duricrusts from those on the LPS. The LI, WII, and the data from Iza et al. (2016) support these findings, as they highlight a high weathering level on the UPS, with a high Th/K ratio and intense lateritization. Table 5 shows the main characteristics of the lateritic duricrusts in the respective geomorphological domains.

## 6. Conclusions

Multisource integration is essential for regolith mapping and should be used as a support tool for regolith field mapping. In this work, the multisource integration was used in the generation of the regolith map



and the reinterpretation of geological units, especially those previously considered to be sedimentary, thus highlighting the following.

- Geochemical associations, such as those related to alkaline and alkaline-earth elements and others related, for example, with Al and Ga, helped to validate the gamma-spectrometric data and to delimit the respective regolithic units. Therefore, the geochemistry was used as another information component for mapping the regolith and confirmed the efficiency of these tools, as they support the identification of areas with different weathering levels.
- It was evident that the integration of geophysical indexes WII, LI, and MI with geochemical data, altimetry, and the relationship between the geochemical weathering indexes (WIP versus CIA) was an efficient method of regolith characterization and mapping. These should be considered broadly useful tools because they can help determine domains with higher or lower weathering intensity.
- The WII highlighted areas with different weathering levels, including those propitious to the occurrence of lateritic duricrusts (high WII and LI) and those with rocks weakly weathered or unaltered. The LI and MI, in addition to integration techniques of multisource data (Iza et al., 2016), are complementary tools and contribute directly to the identification of lateritic duricrusts and their respective parent rocks.

This approach can be confidently applied in areas with difficult access, with restricted access (indigenous and environmental preservation lands) and/or with a lack of detailed maps, and with wide occurrence of lateritic regolith, such as the Brazilian Amazon. The delimitation of domains with higher or lower weathering intensity and with geophysical and geochemical anomalies simultaneously associated with residual or erosional domains is extremely useful for mineral exploration because they can guide geologists to areas with higher or lower interest depending on the mineral resource surveyed. In addition, they can help to reduce time and costs in the mineral prospecting stage. In this sense, the multisource integration and the methodology presented in this paper can be applied to mineral exploration, especially in tropical regions and areas with lateritic regolith predominance.

#### Acknowledgments

The authors thank the CPRM-DIGEOQ for the clearance of the geochemical data and CPRM-DISEGE for the clearance of the aero geophysical data from the Projeto Sudeste de Rondônia, which can be requested by email (sic@cprm.gov.br). The data from CPRM database can be accessed on [www.geosbcprm.gov.br](http://www.geosbcprm.gov.br) or [www.cprm.gov.br](http://www.cprm.gov.br). The authors also thank the Universidade de Brasília (UnB) for the infrastructure. A. M. C. Horbe thanks the Conselho Nacional de Desenvolvimento Científico e Tecnológico (CNPq) for the research scholarship, and I. L. I. E. Herrera thanks the Coordenadoria de Aperfeiçoamento de Pessoal de Nível Superior (CAPES) for the doctorate scholarship.

#### References

- Albuquerque, M. F. D., Horbe, A. M. C., & Botelho, N. F. (2017). Genesis of manganese deposits in southwestern Amazonia: Mineralogy, geochemistry and paleoenvironment. *Ore Geology Reviews*. <https://doi.org/10.1016/j.oregeorev.2017.06.012>
- Anand, R. R., Churchward, H. M., Smith, R. E., Smith, K., Gozzard, J. R., Craig, M. A., & Munday, T. J. (1993). Classification and atlas of regolith landform mapping units—Exploration perspectives for the Yilgarn craton, Australia. CSIRO *Division of Exploration and Mining*, Restricted Report 440R.
- Anand, R. R., & Paine, M. (2002). Regolith geology of the Yilgarn craton, Western Australia: Implications for exploration. *Australian Journal of Earth Sciences*, 49(1), 3–62. <https://doi.org/10.1046/j.1440-0952.2002.00912.x>
- Arhin, E., Jenkin, G. R. T., Cunningham, D., & Nude, P. (2015). Regolith mapping of deeply weathered terrain in savannah regions of the Birimian Lawra Greenstone Belt, Ghana. *Journal of Geochemical Exploration*, 159, 194–207. <https://doi.org/10.1016/j.gexplo.2015.09.008>
- Asghar Calagari, A., Kangarani Farahani, F., & Abedini, A. (2015). Geochemical characteristics of a laterite: The Jurassic Zan deposit, Iran. *Acta Geodynamica et Geomaterialia*, 12(177), 1–11. <https://doi.org/10.13168/AGG.2015.0001>
- Barbosa, I. O., Pires, A. C. B., Lacerda, M. P. C., & Carmelo, A. C. (2013). Geology, airborne geophysics, geomorphology and soils in the individualization of the niquelândia mafic-ultramafic complex, Goiás state, Brazil. *Revista Brasileira de Geofísica*, 31(3), 463–481. <https://doi.org/10.22564/rbgf.v31i3.316>
- Boulangé, B., & Carvalho, A. (1997). The bauxite of Porto Trombetas. In A. Carvalho, B. Boulangé, A. J. Melfi, & Y. Lucas (Eds.), *Brazilian bauxites* (pp. 55–73). São Paulo: USP/FAPESP/ORSTOM.
- Brazil. Departamento Nacional da Produção Mineral. Projeto RADAMBRASIL (1979). *Folha SD.20 Guaporé; geologia, geomorfologia*. Rio de Janeiro: pedologia, vegetação e uso potencial da terra.
- Carranza, E. J. M. (2009). Knowledge-driven modeling prospectivity. In: \_\_\_\_\_. In *Geochemical anomaly and mineral prospectivity mapping in GIS* (Vol. 11, pp. 189–246). Amsterdam: Elsevier. Cap 7.
- Carrier, F., Bourdon, B., Pili, É., Truffert, C., & Wyns, R. (2006). Airborne gamma-ray spectrometry to quantify chemical erosion process. *Journal of Geochemical Exploration*, 88(1-3), 266–270. <https://doi.org/10.1016/j.gexplo.2005.08.053>
- Carrino, T. A., Silva, A. M., Botelho, N. F., & Silva, A. A. C. (2011). Discriminação de áreas de espesso regolito do leste do Estado do Amazonas usando estatística multivariada, algoritmo hiperespectral e modelagem de dados espaciais. *Revista Brasileira de Geofísica*, 29(1), 155–172. <https://doi.org/10.1590/S0102-261X2011000100011>
- Cattell, R. B. (1966). The scree test for the number of factors. *Multivariate behaviour research*, 1(2), 245–276. [https://doi.org/10.1207/s15327906mbr0102\\_10](https://doi.org/10.1207/s15327906mbr0102_10)
- Cohen, D. R., Kelley, D. L., Anand, R., & Coker, W. B. (2010). Major advances in exploration geochemistry, 1998–2007: Geochemistry exploration. *Environment*, 10(1), 3–16. <https://doi.org/10.1144/1467-7873/09-215>
- Cornelius, M., Robertson, I. D. M., Cornelius, A. J., & Morris, P. A. (2007). *Laterite geochemical database for the Western Yilgarn craton, Western Australia*. Perth: Department of Industry and Resources.
- Costa, M. L. (1997). Lateritization as a major process of ore deposit formation in the Amazon region. *Exploration and Mining Geology*, 6(1), 79–104.
- CPRM - Serviço Geológico do Brasil (2006). Projeto Aerogeofísico Sudeste de Rondônia: Relatório final de levantamento e processamento dos dados magnetométricos e gamaespectrométricos. Rio de Janeiro: Lasa Engenharia e Prospecções; Prospectores Aerolevantamentos e Sistemas, 27 v. 1.
- CPRM - Serviço Geológico do Brasil (2016). Banco de dados da CPRM - Geosgb. Accessed in 2016. Disponível em: [www.geosbcprm.gov.br](http://www.geosbcprm.gov.br)

- Craig, M. A. (2001). Regolith mapping for geochemical exploration in the Yilgarn craton, Western Australia. *Geochemistry: Exploration, Environment, Analysis*, 1(2001), 383–390.
- Dauth, C. (1997). Airborne magnetic, radiometric and satellite imagery for regolith mapping in the Yilgarn craton of Western Australia. *Exploration Geophysics*, 28(2), 199–203. <https://doi.org/10.1071/EG997199>
- Dickson, B. L., & Scott, K. M. (1997). Interpretation of aerial gamma-ray surveys—Adding the geochemical factors. *Journal of Australian Geology & Geophysics*, 17(2), 187–200.
- Dury, G. H. (1969). Rational descriptive classification of duricrust. *Earth Science Journal*, 3, 77–86.
- Giorgis, I., Bonetto, S., Giustetto, R., Lawane, A., Pantet, A., Rossetti, P., et al. (2014). The lateritic profile of Balkouin, Burkina Faso: Geochemistry, mineralogy and genesis. *Journal of African Earth Sciences*, 90, 31–48. <https://doi.org/10.1016/j.jafrearsci.2013.11.006>
- Harrison, J. B. (1934). The katamorphism of igneous rocks under humid tropical conditions. In *Imperial bureau of soil science* (pp. 17–31). Harpenden, England: Rothamsted Experimental Station.
- Herrera, I. L. I. E., Iza, E. R. H. F., Filho, E. P. S., Horbe, A. M. C., Santos, S. L. M., & Cabral, L. N. (2017). Técnica Booleana Aplicada à Identificação De Crostas Lateríticas no Sudoeste da Amazônia Brasileira. *Revista Brasileira de Geomorfologia*, 18(2), 411–425. <https://doi.org/10.20502/rbg.v18i2.1182>
- Hill, I. G., Worden, R. H., & Meighan, I. G. (2000). Geochemical evolution of a palaeolaterite: The Interbasaltic formation, northern Ireland. *Chemical Geology*, 166(1–2), 65–84. [https://doi.org/10.1016/S0009-2541\(99\)00179-5](https://doi.org/10.1016/S0009-2541(99)00179-5)
- Hill, I. G., Worden, R. H., & Meighan, I. G. (2001). Formation of interbasaltic laterite, horizons in NE Ireland by early Tertiary weathering process. *Proceedings of the Geologists Association*, 112(4), 339–348. [https://doi.org/10.1016/S0016-7878\(01\)80013-4](https://doi.org/10.1016/S0016-7878(01)80013-4)
- Inpe – Instituto Nacional de Pesquisas Espaciais, 2018. Retrieved from <http://tempo.cptec.inpe.br/>
- Isles, D., & Rankin, L. (2000). *Geological interpretation and exploration targeting from aeromagnetic data. Workshop*. Brasília, DF: ADIMB.
- Iza, E. R. H. F., Horbe, A. M. C., & Silva, A. M. (2016). Boolean and fuzzy methods for identifying lateritic regoliths in the Brazilian Amazon using gamma-ray spectrometric and topographic data. *Geoderma*, 269, 27–38. <https://doi.org/10.1016/j.geoderma.2016.01.037>
- Kaiser, H. F. (1958). The varimax criterion for analytic rotation in factor analysis. *Psychometrika*, 23(3), 187–200. <https://doi.org/10.1007/BF02289233>
- Kotschoubey, B., Calaf, M. J. C., Lobato, A. C. C., Leite, A. S., & Azevedo, C. H. D. (2005). Caracterização e gênese dos depósitos de bauxita da provincial bauxitífera de Paragominas, Noroeste da Baía do Grajaú, Nordeste do Pará/Oeste do Maranhão. In O. J. Marini, E. T. Queiroz, & B. W. Ramos (Eds.), *Caracterização de depósitos minerais em distritos mineiros da Amazônia* (pp. 691–782). Brasília-DF: ADIMB.
- McBratney, A. B., Mendonça Santos, M. L., & Minasny, B. (2003). On digital soil mapping. *Geoderma*, 117(1–2), 3–52. [https://doi.org/10.1016/S0016-7061\(03\)00223-4](https://doi.org/10.1016/S0016-7061(03)00223-4)
- Minty, B. (2011). Short note: On the use of radioelement ratios to enhance gamma-ray spectrometric data. *Exploration Geophysics*, 42(1), 116–120. <https://doi.org/10.1071/EG10011>
- Moreira, F. R. S., Almeida-Filho, R., & Camara, G. (2003). Spatial analysis techniques applied to mineral prospecting: An evaluation in the Poços de Caldas plateau. *Revista Brasileira de Geociências*, 33(2), 183–190. <https://doi.org/10.25249/0375-7536.20033352183190>
- Nesbitt, H. W., & Young, G. M. (1982). Early Proterozoic climates and plate motions inferred from major element chemistry of lutites. *Nature*, 299(5885), 715–717. <https://doi.org/10.1038/299715a0>
- Oliveira, S. B., Costa, M. L., & Filho, H. J. P. (2016). The lateritic bauxite deposit of Rondon do Pará: A new giant deposit in the Amazon region, northern Brazil. *Economic Geology*, 111(5), 1277–1290. <https://doi.org/10.2113/econgeo.111.5.1277>
- Parker, A. (1970). An index of weathering for silicate rocks. *Geological Magazine*, 107(06), 501–504. <https://doi.org/10.1017/S0016756800058581>
- Pires, A. C. B., & Moraes, R. A. V. (2006). New processing technologies applied do airborne geophysical data: Impact on interpretation. // *Simpósio Brasileiro de Exploração Mineral – Simexmin*. Ouro Preto, Minas Gerais-Brasil.
- Quadros, M. L., Do, E. S., & Rizzotto, G. J. (2007). *Geologia e recursos minerais do Estado de Rondônia: texto explicativo do mapa geológico e de recursos minerais do Estado de Rondônia-escala 1:1.000.000*. Porto Velho: CPRM. Programa Geologia do Brasil-PGB.
- Reimann, C., Filzmoser, P., Garret, R., & Dutter, R. (2008). *Statistical data analysis explained: Applied environmental statistics with R*. Chichester: John Wiley. <https://doi.org/10.1002/9780470987605>
- Roest, W. R., Verhoef, J., & Pilkington, M. (1992). Magnetic interpretation using the 3-D analytic signal. *Geophysics*, 57(1), 116–125. <https://doi.org/10.1190/1.1443174>
- Schellman, W. (1981). Considerations on the definition and classification of laterites. Proc. Int. Seminar on Lateritisation Processes. Trivandrum, Proceedings, 1–10.
- Schellmann, W. (1983). A new definition of laterite. *Geological Survey of India, Memoirs*, 120, 1–7.
- Tardy, Y. (1993). *Pétrologie des latérites et des sols tropicaux*. Paris: Masson.
- Taylor, R. S., & McLennan, S. M. (1985). *The Continental Crust: Its Composition and Evolution*. Blackwell, Oxford.
- Wedepohl, K. H. (1969). *Handbook of geochemistry*. Berlin: Springer-Verlag.
- Wilford, J. (2012). A weathering intensive index for the Australian continent using airborne gamma-ray spectrometry and digital terrain analysis. *Geoderma*, 183–184, 124–142. <https://doi.org/10.1016/j.geoderma.2010.12.022>
- Wilford, J. R., Bierwirth, P. N., & Craig, M. A. (1997). Application of airborne gamma-ray spectrometry in soil/regolith mapping and applied geomorphology. *Journal of Australian Geology & Geophysics*, 17(2), 201–216.
- Wimpenny, J., Gannoun, A., Burton, K. W., Widdowson, K., James, R. H., & Gislason, S. R. (2007). Rhenium and osmium isotope and elemental behaviours accompanying laterite formation in the Deccan region of India. *Earth and Planetary Science Letters*, 261(1–2), 239–258. <https://doi.org/10.1016/j.epsl.2007.06.028>
- Xiao, W., Hongbing, J., Shijie, W., Huashuo, C., & Changshun, S. (2014). The formation of representative lateritic weathering covers in south-central Guangxi (southern China). *Catena*, 118, 55–72. <https://doi.org/10.1016/j.catena.2014.01.019>